JOURNAL OF SPACECRAFT AND ROCKETS
Vol. 40, No. 2, March–April 2003

Total Densities Derived from Accelerometer Data

Sean Bruinsma* and Richard Biancale†
Centre National d'Etudes Spatiales, 31401 Toulouse, France

The German satellite Challenging Minisatellite Payload (CHAMP), carrying the STAR accelerometer onboard, was launched in July 2000. The CHAMP mission profile is compatible with studies of the thermosphere: it will provide good geographical and altitude coverage over a period of five years. The preprocessing of the accelerometer data consists of correcting them for maneuvers, specific events, and instrumental bias. The total density can then be reconstituted, employing a model for the aerodynamic coefficient. We have employed a theory based on diffuse reemission applied to a 15-plate macromodel. The accuracy of the observed densities depends mainly on the uncertainties of the estimated accelerometer calibration parameters and of the aerodynamic coefficient, as well as on geomagnetic activity. The six weeks of data analyzed in this preliminary study showed their high precision and model shortcomings. Assimilation of at least one year of data in a thermosphere model will significantly increase its accuracy, which, in turn, will improve satellite drag modeling.

Nomenclature

A	=	area
a	=	acceleration
a_p	=	planetary geomagnetic activity index, nT
C_D	=	drag coefficient
$F_{10.7}$	=	index of solar radio flux at 10.7 cm
K_d	=	diffuse reflectivity coefficient
K_p	=	scaled planetary geomagnetic activity index
K_s	=	specular reflectivity coefficient
Mg II	=	index of solar flux at 280 nm
N	=	direction perpendicular to the orbit plane
R	=	direction Earth center of mass to satellite
T	=	direction of flight
T_{atmo}	=	kinetic temperature of ambient gas, K
T_{sat}	=	temperature of satellite surface, K
u	=	incident gas atom to surface atom mass ratio
v	=	speed with respect to the atmosphere (m/sec)
α	=	accommodation coefficient
ρ	=	density, kg/m^3
σ	=	standard deviation
ϕ	=	incidence angle between satellite surface and speed

Subscripts

alb	=	acceleration; Earth albedo
drag	=	acceleration; atmospheric drag
IR	=	acceleration; Earth infrared radiation
sol	=	acceleration; solar radiation pressure
tot	=	acceleration; total effect

Superscripts

i	=	surface i of the CHAMP macromodel
model	=	acceleration; model computation
STAR	=	acceleration; STAR measurement

Introduction

THE German satellite Challenging Minisatellite Payload (CHAMP) was launched in a circular, nearly polar orbit at 460 km altitude in July 2000. The two main mission objectives are the mapping of the magnetic and gravity fields of the Earth. Another, secondary objective concerns the monitoring of atmospheric density, which is the subject of the present study. The STAR accelerometer developed by the Office National d'Etudes et de Recherches Aerospatiales (ONERA), placed at the center of gravity of CHAMP, measures the nongravitational accelerations acting on it. The atmospheric drag perturbation causes the largest signal, which is mainly projected on the along-track component. It can be retrieved by accurately modeling the direct (solar) and indirect [terrestrial albedo and infrared (IR)] radiation pressure forces and subsequently removing them from the measurement.

The CHAMP mission profile is particularly interesting for upper-atmosphere studies: it provides good geographical coverage over a period of five years. The 87-deg orbit inclination ensures a nearly complete latitudinal coverage, whereas the solar local time is completely sampled (0–24 h) approximately every four months. The initial altitude in July 2000 was 460 km, but, as a result of natural decay and orbit altitude corrections if necessary, it will be 200 km at the end of the five-year mission. Over that period of time, the same instrument will cover the solar activity from maximum (2000–2001) to minimum (2005) conditions. This is important taking the heterogeneity of the density database available nowadays into account. Assimilation of the CHAMP data in a thermosphere model such as Drag Temperature Model (DTM) will probably significantly increase its accuracy (currently at the 20% 1σ level). This, in turn, will improve satellite drag modelling, leading to more accurate and less parameterized orbit computations.

The preprocessing of the accelerometer measurements is done in three stages:

1) The spikelike accelerations are removed from the measurements. The spikes are partly caused by orbit attitude maneuvers (approximately 100/day), whereas others have been identified as being caused by parasite electric currents.

2) The data are smoothed using a low-pass filter with cutoff period of 10 s, and small data gaps are filled by interpolation.

3) The preprocessed accelerometer observation is obtained by applying the instrumental biases and scale factors determined in the calibration/validation phase.

The density is derived from the tangential component of the measured nongravitational acceleration only. The data preprocessing for density retrieval is slightly different than for orbit computation: all spikelike accelerations, also those caused by orbit attitude maneuvers (approximately 100/day), are removed from the measurements.

The first step in the density retrieval procedure consists in removing that part of the acceleration from the data that is not caused by drag. The acceleration as a result of the direct solar radiation and Earth/moon shadowing is accurately modeled, using a calibrated shadow function based also on the accelerometer observations. By numerically integrating discrete surface elements visible to the

Received 3 January 2002; revision received 9 October 2002; accepted for publication 2 December 2002.

*Research Engineer, Department of Terrestrial and Planetary Geodesy; sean.bruinsma@cnes.fr.

†Research Engineer, Department of Terrestrial and Planetary Geodesy.

spacecraft and using daily albedo maps derived from observed flux at the top of the atmosphere, the acceleration caused by the satellite-intercepted flux is modeled as accurately as possible. The acceleration caused by observed terrestrial IR radiation is modeled in a similar way. The reflectivity coefficients of CHAMP for both short-wave (visible) and long-wave (IR) radiation have been measured on the ground. After removal of the just-mentioned accelerations from the measured one, the drag signal remains.

In the second step the total atmospheric density is reconstituted. The accuracy of this calculation depends mainly on the uncertainty in the estimated accelerometer calibration parameters, the aerodynamic drag coefficient, and the unknown thermospheric winds. The density data have been compared with semi-empirical thermosphere models, such as DTM-94,[1] DTM-2000,[2] and MSIS-86[3] (mass spectrometer and incoherent scatter). These models are based on the hypothesis of independent static diffuse equilibrium. They reproduce total and partial densities as a function of altitude, latitude, solar local time, and solar and geomagnetic activity. The integration of the differential equation of diffuse equilibrium leads to the height distribution of the constituents, whereas the variations are modeled using a spherical harmonic expansion. The model variations result from a least-squares fit to total density, mass spectrometer, and temperature data. At 460 km atomic oxygen is the major constituent. The comparison allows an evaluation of the model predictions primarily of that constituent and of the temperature indirectly. The CHAMP data are also used to compare the solar activity proxy-indicator $F_{10.7}$ (solar radio flux) with the *Mg* II index,[4] which has been used in the construction of DTM-2000.

The next section gives an overview of the CHAMP satellite and its mission profile from the viewpoint of thermospheric studies. It is followed by sections describing the density retrieval procedure and the error budget. A first density data analysis as well as a comparison to three atmospheric density models is presented, and the paper ends with a conclusion and prospects.

Satellite and Mission Profile in Perpspective

The CHAMP mission, proposed by the GeoForschungsZentrum Potsdam, was decided on in 1995 by the German space agency Deutsches Zentrum für Luft- und Raumfahrt. It is mainly dedicated to the study of the Earth's magnetic and gravity fields, whereas its potential contribution to the modeling of the neutral upper atmosphere, using the accelerometer data, was only recognized at a later stage. Figure 1 shows the satellite, with the magnetometers fixed to the boom, and the digital ion driftmeter fixed to the front panel. The nominal satellite attitude is with the boom aligned with the tangential component of the radial, tangential, and normal (RTN) directions local satellite frame, thus close to the velocity vector. This attitude is maintained within 2 deg by thruster activity.

The good geographical coverage of the data, thanks to the 87-deg orbit inclination and the complete sampling of solar local time every four months approximately, are important improvements over (older) data sets such as CACTUS.[5] That accelerometer (equally developed by ONERA) flew on the French CASTOR satellite and provided a total density data set from 1975 to 1978. However, the orbit inclination of 30 deg severely limited its coverage. The launch of CHAMP during the solar cycle maximum, and considering its nominal mission lifetime of five years, is advantageous also because it ensures a good sampling of solar activity. The sun's activity will vary from maximum (2001–2002) via the entire decaying phase of solar cycle 23 to almost minimum conditions (2005). The CHAMP density data set will be more complete than that of CACTUS and most other available ones in this respect also because these were obtained under either high or low solar activity. This long observation period equally allows a good determination of annual and semiannual variations in the upper atmosphere.

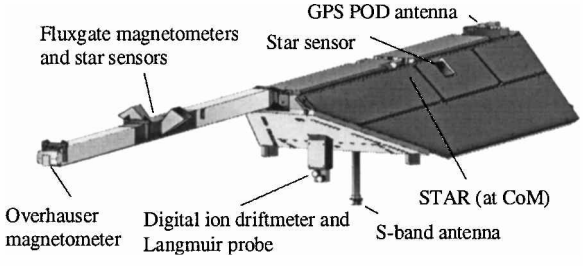

Fig. 1 CHAMP satellite and its scientific payload.

The mean altitude in July 2000 was 460 km, but it will be 200 km at the end of the five-year mission as a result of natural decay and possibly orbit altitude corrections. This implies an increasing atmospheric drag encountered over the mission of approximately two orders of magnitude (DTM-94 estimate), not taking the decreasing solar activity into account. It will also profoundly change the atmospheric composition: at 460 km altitude oxygen is the main constituent, whereas at the end of the mission oxygen and molecular nitrogen will be the main constituents. Although this has no consequence for the present preliminary study, it does limit the use of the data set for modeling purposes. Only total density can be obtained from accelerometer measurements, and from these observations one can only extract main atmospheric constituents. Only mass spectrometer data give direct information on the atmospheric composition. However, matters are complicated for these observations because of different instrumental scale factors that have to be estimated for each constituent.

Density Retrieval Procedure

Preprocessing of the Accelerometer Data

The raw accelerometer data have to be preprocessed in order to eliminate all spurious signals not caused by nongravitational or thruster forces, as well as to fill small data gaps. The derived density is proportional to the measured acceleration, and so spurious signals result in erroneous densities. The data gaps smaller than two minutes are filled because the orbit determination software we use requires continuous measurements.

The satellite attitude maneuvers cause a significant signal on the tangential accelerometer axis. This is caused mainly by misalignment of the thruster pairs, causing translation besides the desired pure rotation around the center of mass. These accelerations, with duration up to 3 s, are filtered from the data in this analysis. After the preprocessing stage the data should only contain nongravitational signal.

Nongravitational Force Modeling

The accelerometer measures the nongravitational surface accelerations acting on the satellite in the three directions RTN, and so the dynamical modeling of the orbital motion only requires gravitational force models. To isolate the atmospheric drag component from the total observed acceleration, it is nonetheless necessary to have the disposal of accurate solar and terrestrial radiation pressure force models. The accuracy of these models is determined by the provided reflectivity coefficients and areas of the different satellite panels (for visible and IR wavelengths), measured on ground by the constructor, as well as knowledge pertinent to terrestrial albedo and IR emissivity.

In this study the applied CHAMP macromodel consists of 15 plates, for which accurate areas are known from Daimler–Benz Aerospace. They measured the (mean) reflectivity coefficients of each plate and specified the material(s). Table 1 presents the macromodel elements used in this study. However, some of these values are not accurate because some parts of the satellite were subsequently (partly) covered with thermal foil.

Terrestrial albedo and emissivity top-of-atmosphere observations are collected by the European Centre for Medium-Range Weather Forecast and were made available to us in the form of 6-hourly 0.5×0.5 deg grids. The Earth radiation pressure force is computed using the model described by Knocke et al.,[6] in which the satellite's cone of visibility of the Earth's surface is first divided into discrete segments. We calculate the Earth's albedo effect with 100 segments under the satellite, equally spaced within 10 concentric circles, representing the total satellite-intercepted flux. Moreover, each segment produces the same acceleration on a spherically shaped satellite in case of a uniform albedo and emissivity. The incremental acceleration caused by diffuse short-wave and long-wave radiation

Table 1 CHAMP macromodel

Panel	Area, m^2	K_s (visible)	K_d (visible)	K_s (IR)	K_d (IR)	Material
Top	1.2920	0.05	0.30	0.03	0.16	SiO_2
Bottom	3.6239	0.68	0.20	0.19	0.06	Teflon®
Left	3.1593	0.05	0.30	0.03	0.16	SiO_2
Left (rear)	0.3020	0.40	0.26	0.23	0.15	Kapton/SiO_2
Right	3.1593	0.05	0.30	0.03	0.16	SiO_2
Right (rear)	0.3020	0.40	0.26	0.23	0.15	Kapton/SiO_2
Aft	0.4902	0.40	0.26	0.23	0.15	Kapton/SiO_2
Front	1.2199	0.20	0.40	0.26	0.51	Sandblasted Al
Boom (top)	0.5110	0.40	0.26	0.23	0.15	Kapton/SiO_2
Boom (top)	0.4190	0.64	0.20	0.71	0.22	Kapton/Al
Boom (bottom)	0.9300	0.40	0.26	0.23	0.15	Kapton/SiO_2
Boom (left)	0.9300	0.40	0.26	0.23	0.15	Kapton/SiO_2
Boom (right)	0.9300	0.40	0.26	0.23	0.15	Kapton/SiO_2
Front	0.0880	0.20	0.40	0.26	0.51	Sandblasted Al
Front	0.1314	0.40	0.26	0.23	0.15	Gold foil

from each segment for each face of the macromodel in view of the Earth is computed using Lambert's law of diffuse radiation, assuming that each segment can be approximated as a plane surface tangent to the center of the segment. The total acceleration is obtained through summation over the segments and the macromodel surfaces. The solar radiation pressure force, with Earth- and moon-shadowing effects, is computed using a regularizing shadow function, calibrated to the CHAMP orbit, and taking the variation of the solar constant (4.5605×10^{-6} N/m^2 at 1 astronomical unit) over the Earth orbit about the sun into account.

The general expression for the atmospheric drag acceleration is as follows:

$$a_{\text{drag}} = -\tfrac{1}{2} C_D (A/m) \rho v^2 \tag{1}$$

where the satellite speed is computed relative to the atmosphere, which is assumed to be corotating with the Earth. This assumption is valid when the wind speeds are negligible compared to the satellite speed, that is, when the geomagnetic activity is low. The drag coefficient, which gives a measure of the momentum exchange between the satellite surface and the colliding particles, is modeled under the assumptions of hyperthermal free-molecular flow and accommodated diffuse reemission of the neutral atmospheric particles according to Cook.[7] The first assumption is based on the value of the molecular speed ratio (satellite speed/most probable molecular speed), which is always larger than five for CHAMP. Therefore, we can neglect the random thermal motion of the atmospheric molecules, that is, we consider the flow as hyperthermal. Experiments have shown that the reemission mechanism is dependent on surface temperature: it was found to be diffuse for a surface at room temperature, whereas it was nearly completely specular for a very hot surface of 1600 K. Because the most probable mean satellite surface temperature is approximately 273 K, the diffuse model is appropriate. The expression of the drag coefficient for flat plate i ($i = 1, 15$) of the macromodel at incidence ϕ^i to the flow is

$$C_D^i = 2\left[1 + \tfrac{2}{3}\sqrt{1 + \alpha^i \left(T_{\text{sat}}^i / T_{\text{atmo}} - 1\right)} \sin\phi^i\right]$$

$$\alpha^i = 3.6 u^i / (1 + u^i)^2 \tag{2}$$

The values of T_{atmo} and the mean mass of the gas are predicted by an atmospheric density model. These values have an accuracy of 6 and 20%, respectively, in case of the DTM-2000 model and slightly worse when using DTM-94 or MSIS-86. The effective cross-sectional area perpendicular to the velocity vector and the incidence angles are computed accurately using the 15-plate macromodel correctly oriented by the telemetered attitude quaternions. The satellite mass history is monitored and decreased 0.22 kg over the period considered in this study (24 September–7 November 2000). The density value is predicted using a model such as DTM or MSIS and proportional to the measured acceleration.

Orbit Determination

Orbit determination is necessary to this study in order to calculate the STAR measurements with respect to the Earth (altitude, latitude, local time). The predicted nongravitational accelerations are computed simultaneously. CHAMP precise orbit computation is ensured by the global positioning system (GPS) and satellite laser ranging (SLR) tracking systems, complemented by attitude information, thanks to star sensors, in the form of quaternions to orient the macromodel in inertial space. The CHAMP tracking and accelerometer data were processed using the GINS orbit determination software at Centre National d'Etudes Spatiales/Groupe de Recherche en Géodésie Spatiale Toulouse. Data used came from the period 24 September through 7 November 2000 (day-of-year 268 through 312). Because of several data gaps caused by GPS data unavailability and STAR-software uploads, 21 arcs of 1 to 1.5 days in length, totalling 29 days of processed data, were computed over that period. The adjusted parameters in each arc included the initial state vector, CHAMP GPS-clock biases per 30 s, GPS ambiguities per pass, and the bias and scale factor of the radial component of the accelerometer as a result of a malfunction of that axis. The International GPS Service provided the precise orbits and clock parameters of the GPS satellites.

The typical rms of an orbit adjustment (with STAR observations) is at the 80-cm, 1.5-cm, and 30-cm level for GPS pseudorange, phase, and SLR residuals, respectively, when we use the GRIM5-CHAMP gravity model[8] up to degree and order 120. These numbers are 350, 4, and 100 cm, respectively, when using GRIM5-S1.[9] In this specific study, which is aimed at total density retrieval, the orbit precision requirements are not stringent, and both just-mentioned gravity fields yield satisfactory results. Each accelerometer measurement, and thus each derived density, is linked to the satellite position at epoch. Because the upper atmosphere models have a low resolution (<2 deg), this condition is easily met. A dedicated output file was created containing all necessary parameters, updated each integration step, for subsequent density calculation and analysis purposes. These parameters are Julian date, the tangential components of the observed (preprocessed STAR) and modeled nongravitational accelerations (drag and solar and terrestrial radiation pressure), altitude (above GRS-80 ellipsoid), geocentric latitude, solar local time, longitude, mean and daily solar radio flux, and the planetary geomagnetic index K_p.

Total Density Computation

The "observed" total density ρ^{STAR} is computed by scaling of the modeled density ρ^{model} using only the tangential components of measured and modeled accelerations as follows:

$$\rho^{\text{STAR}} = \frac{a_{\text{total}}^{\text{STAR}} - a_{\text{sol}}^{\text{model}} - a_{\text{albedo}}^{\text{model}} - a_{\text{IR}}^{\text{model}}}{a_{\text{drag}}^{\text{model}}} \rho^{\text{model}} \tag{3}$$

In this equation the total tangential acceleration measured by STAR, corrected for the instrumental bias and corresponding scale factor, represents the sum of the surface accelerations acting on CHAMP. The determination of the tangential component of the measured drag acceleration is achieved by accurately modeling the radiation

pressure forces and subtracting their tangential components. The ratio of the observed (corrected STAR measurement) to the modeled [Eq. (1)] drag acceleration is the scale factor of the predicted density.

A density observation is calculated at each integration step applying this procedure. For practical reasons a step size of 30 s, corresponding to an observation approximately every 250 km along the arc, has been chosen in this first analysis. This resolution will be enhanced by a factor of two to three when one year of CHAMP/STAR observations for modeling purposes will be processed. The 29 days of processed data produced around 79,000 density observations. Some arcs were computed with a small step size of 4 s for specific analyses, which will be presented in the Data and Model Evaluation section.

Error Budget

The total density derived from STAR measurements and model predictions is affected by errors that will be discussed next in order of importance. These errors can be divided into two groups: errors causing (mainly) a systematic offset of the observations with respect to their absolute values and errors affecting their instantaneous noise level.

The uncertainty in the instrumental calibration parameters (bias and scale factor) causes a systematic error. In this study the following calibration parameters[8] were used for the tangential component: a bias of -3.075×10^{-6} m $\cdot$ s^{-2} and a scale factor of 0.82. These parameters were estimated simultaneously with gravity field spherical harmonic coefficients during the calibration activities.[8] Analysis of STAR data in June and July 2001 confirmed the determined values of the tangential bias and scale factor to better than 10%.

The second significant systematic error source is caused by the modeled drag coefficient, which directly affects the value of the reconstituted density, as can be seen in Eq. (1). The accuracy of the formula is approximately at the 5–10% level because of the validity of the hyperthermal flow regime assumption at the altitude of CHAMP. Its accuracy then mainly depends on the quality of the used density model (for temperature and mean mass) and knowledge of the satellite surface materials and their temperature evolutions over the orbit, as can be seen in Eq. (2). The value α is not very sensitive to errors in the mass ratio u; errors of the order of 20% in u modify it by approximately 1%. The atmospheric kinetic temperature is accurate at the 6% level, which error would modify the drag coefficient and thus the density by approximately 1%. The mean and varying components of the satellite surface temperatures are not known; an error in the mean temperature causes a systematic offset of the calculated density, whereas the varying part (caused by shadowing) causes a day–night signature. The mean value of 273 K is based on the thermal model of the French SPOT satellites. That model predicts large temperature variations of the order of 100 K for the solar panel: 213 K in the shadow and 328 K when sunlit. Fortunately, the sensitivity of the drag coefficient with respect to the satellite temperature is also small, causing errors of less than 2%.

The minimum or instrumental noise level of the observations is determined by the accelerometer's tangential sensitivity of 3×10^{-9} m/s^2/Hz$^{1/2}$ in the measurement bandwidth (10^{-4}–10^{-1} Hz) and is at the 1–3% level. The single most important factor determining the noise in the observations has geophysical origin and is caused by the neutral winds. These winds can be significantly different from the case of a corotating atmosphere, which we assumed here [see Eq. (1)], in particular during geomagnetic storms.[10] They cannot be accurately separated from the retrieved densities because thermospheric wind models have large uncertainties and give mean, qualitative predictions. The maximum error occurs when the wind is directed along the satellite velocity vector, along the accelerometer's tangential axis, and amounts to approximately 5% per 200 m/s. The strongest winds are encountered at high latitudes during geomagnetic storms, when they attain 600–1000 m/s, but they become large (200 m/s) even down at tropical latitudes. These values have been obtained from the Thermosphere General Circulation Model [output available at the Coupling, Energetics, and Dynamics of Atmospheric Regions database (CEDAR)], whose model is consistent with observed upper atmosphere winds. There are several geomagnetic storms during the observational period, with a_p/K_p up to $154/7^-$, and so the maximum geophysical noise during those periods is at approximately the 20% level at high latitudes and 5% elsewhere. There are two days with a_p/K_p values larger than 111/6, which constitutes less than 6% of the data set. For periods where a_p/K_p is less than $32/3^+$, which is true for 70% of the density observations, these noise numbers are 5 and 2%, respectively. The remaining contributions to the noise are negligible. These are caused by attitude errors, errors in the modeled radiation pressure accelerations, and the mass history of the spacecraft. The attitude control error is smaller than 0.1 deg. The tangential component of the combined radiation pressure forces is two orders of magnitude smaller than the drag force, and so modeling errors have a very small effect. The mass is monitored and available in the housekeeping data; it decreased from 521.61 to 521.39 kg over the studied period. Table 2 summarizes the contributions to the error budget. The total uncertainty in the absolute value of the reconstituted density is estimated at 15–25%, depending on the geomagnetic activity.

Table 2 Error budget of the retrieved densities

Contribution	Systematic offset (uncertainty)	Noise
STAR calibration	10%	——
Drag coefficient	5–10%	1%
STAR resolution	——	1–3%
Winds $-K_p < 3^+$	——	2–5%
$-K_p > 6^-$	——	5–20%
Area-to-mass ratio	——	0%
Reflectivity coefficients	——	0%
Data preprocessing	——	Residual spikes

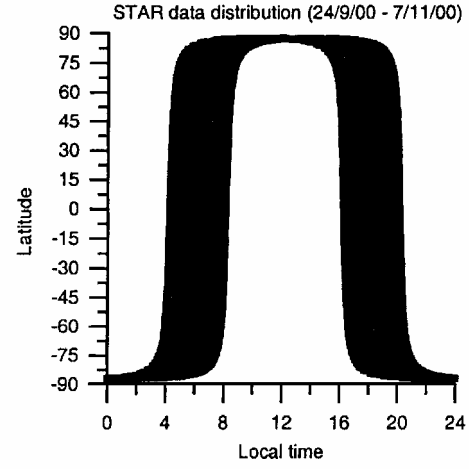

Fig. 2 STAR latitude/local time data distribution.

Data and Model Evaluation

The observations during the period 24 September–7 November provide homogeneous latitude coverage between -87 and 87 deg in the 419–500-km-altitude range. The local time coverage on the other hand, which drifts counterclockwise, is not complete, as can be seen in Fig. 2. The mean solar radio flux (flux averaged over three solar rotations of 27 days) was stable with 175.1 ± 4.7 solar flux units on the average, whereas the mean geomagnetic activity was 2^+ for the six-week period. The noise level of the derived densities is consistent with the STAR specifications, namely a noise of 3–5% during density minima (night) and less than 0.5% during the maxima (day). Although the data noise is much below the current modeling accuracy of approximately 20% (1σ), switching the instrument to a higher numerical resolution for analysis purposes is recommended. The preprocessing of the raw accelerometer data is not yet at the aimed precision level because spikes are not completely removed. Figure 3 shows an example of a residual peak in the data, as well as of the noise level.

To evaluate the additional information in the STAR-derived densities with respect to the predicted model densities, we have first computed power spectra using the periodogram method for unevenly spaced observations.[11] Figures 4a–4d display the power spectra

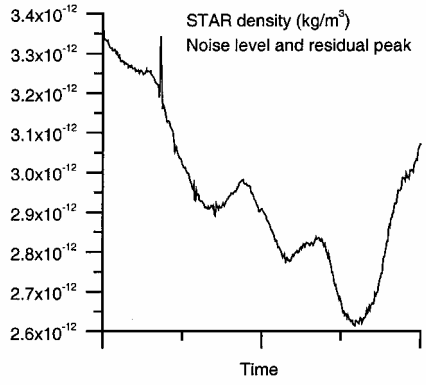

Fig. 3 STAR-density data noise.

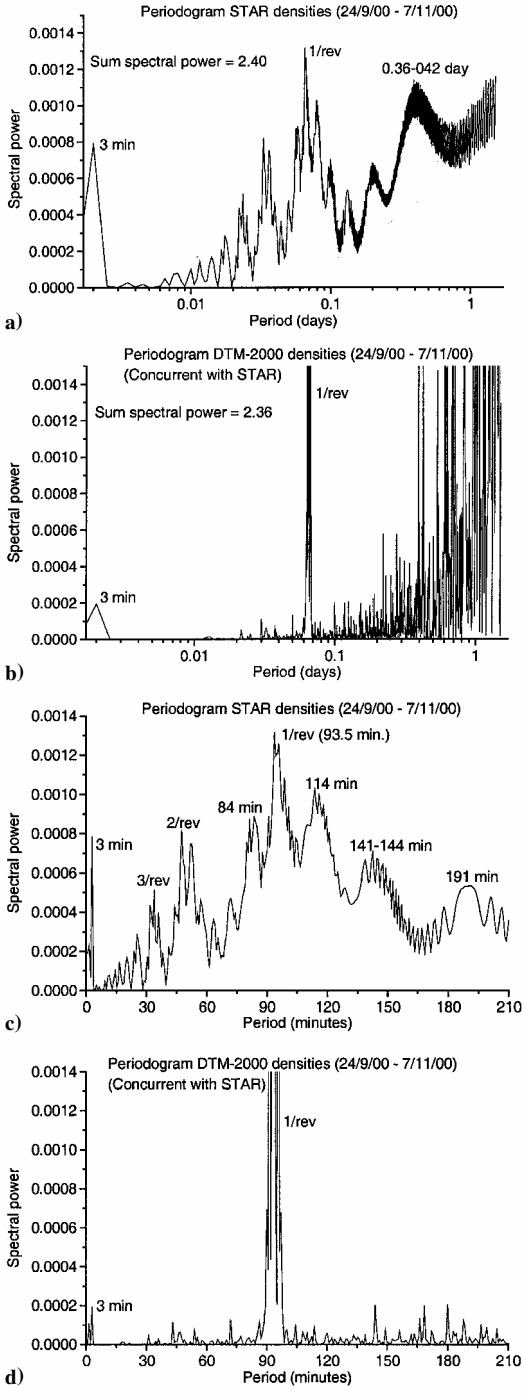

Fig. 4 Periodograms of the STAR densities (a and c) and the densities predicted with DTM-2000 (b and d). Figures 4c and 4d are enlargements of Figs. 4a and 4b, respectively.

of the observations and the corresponding DTM-2000 predictions, where Figs. 4c and 4d are enlargements of Figs. 4a and 4b, respectively. The power spectral densities can be directly compared because the same time interval and the same number of data were analyzed. The summed amplitudes of Figs. 4a and 4b are equivalent and so verify this. Although it is impossible to interpret all signals the power spectra reveal, several of them can be partly explained. Both the periodogram of the observations and that of the predictions have the largest amplitudes around the orbital frequency (1/rev) of approximately 93.5 min. However, the density model produces a narrow series of peaks with amplitudes 20 times larger than the broad peak produced by the observed densities. Second, no significant signals are present in the model below the 1/rev frequency, whereas the spectrum of the observed densities shows 2/rev and 3/rev signals, as well as signals at lower frequencies. The side lobes about the 1/rev peak in Fig. 4c, with periods of approximately 84 and 114 minutes, are artifacts of the periodogram method caused by data noise. This has been verified by simulation.

The differences between the spectra are a clear indication of inadequate density modeling. Moreover, it demonstrates that estimating sinusoidal empirical 1/rev accelerations in precise orbit determination only absorb part of the orbit error. The variability of the upper atmosphere as a result of solar radiation and auroral effects and the gravity waves and high-amplitude winds they provoke constitute major sources of geophysical noise in density modeling. These features are not captured in present-day models and will probably only be represented in a qualitative way in the future.

The differences between modeled and observed density have been analyzed qualitatively by comparing densities from individual orbits under low and high geomagnetic activity conditions. An example of these comparisons is given in Fig. 5, which displays the observed and predicted densities for two orbits in November 2000 (Figs. 5a and 5c), with $K_p = 0^+$ and 6, respectively. The observed-to-predicted ratio (O/C) is often used in density modeling instead of the usual residual O-C, and these quantities are displayed in Figs. 5b and 5d, respectively. These figures demonstrate, in an instantaneous way, the modeling deficiencies revealed by the periodograms as a function of geographical position. The density behaves qualitatively as expected under low and high geomagnetic activity; the resulting time series are smooth (Fig. 5a) and erratic (Fig. 5c), respectively. However, even when there are only very small geomagnetic disturbances the model reproduces density with significant biases, which is shown in Fig. 5b. These are largest on the night side (4–6 hrs local time) and are caused by a latitudinal gradient that is too small. The day-side modeling is better, but the two large bumps in Fig. 5b indicate that the subsolar bulge does not have the correct form or phase. The mean value of the residuals is 0.98, which is misleading when their rms is not given as well; and even when it is given, it cannot be used to detect systematic modeling errors. During a geomagnetic storm, the densities are increased down to low, tropical latitudes caused by the storm energy input. In this example the increase amounts to approximately 25%. Several large peaks are observed within the auroral oval (|60–80| deg), and these are clearly a function of latitude and local solar time and/or longitude (Figs. 5b and 5d). The peaks, with relative amplitudes of 20–60%, are not seen in predicted densities because of the limitations of the modeling algorithm. First, the latitudinal model terms are represented by Legendre polynomials, and these must be calculated to a too high degree to reproduce the fast variations at high latitudes, creating numerical instabilities caused by inadequate data. Second, the geomagnetic index K_p is more representative of disturbances at auroral latitudes than at the poles.[12] Moreover, because it is a planetary index it does not give information per hemisphere or as a function of local time.

The accuracy of the derived densities decreases with increasing geomagnetic activity as a result of the ever-larger winds that alter the computed satellite speed with respect to the atmosphere. The density profiles shown in Fig. 5, for example, can be significantly erroneous there where the variations are largest, so close to the magnetic poles. In case of a wind converging to the pole, the satellite will encounter a change in the sign of the wind for example, leading to a systematic effect in the derived density. This has been quantified in the error budget given in Table 1. We have employed HWM90[13] (Horizontal

Table 3 Modeling performance of DTM-2000, DTM-94, and MSIS-86, given as the mean and rms of the residuals (O/C), compared with accelerometer and mass spectrometer data sets (mean $F_{10.7}$, altitude, and latitude coverages of the data are given in the last three columns)

Data set	DTM-2000	DTM-94	MSIS-86	$F_{10.7}$	Altitude, km	Latitude,°
STAR	1.17; 0.31	1.18; 0.28	1.20; 0.29	170; 180	420; 500	−87; 87
DE-2 (O)[a]	1.00; 0.19	0.97; 0.18	0.97; 0.19	150; 230	225; 600	−90; 90
DE-2 (N_2)[a]	1.02; 0.26	0.92; 0.26	0.94; 0.29	150; 230	225; 400	−90; 90
CACTUS[b]	0.98; 0.19	0.96; 0.19	1.00; 0.19	65; 80	225; 500	−30; 30

[a]DTM-2000, DTM-94, and MSIS-86 assimilated these data sets, but with different instrumental bias factors.
[b]Data assimilated by DTM-2000 and DTM-94.

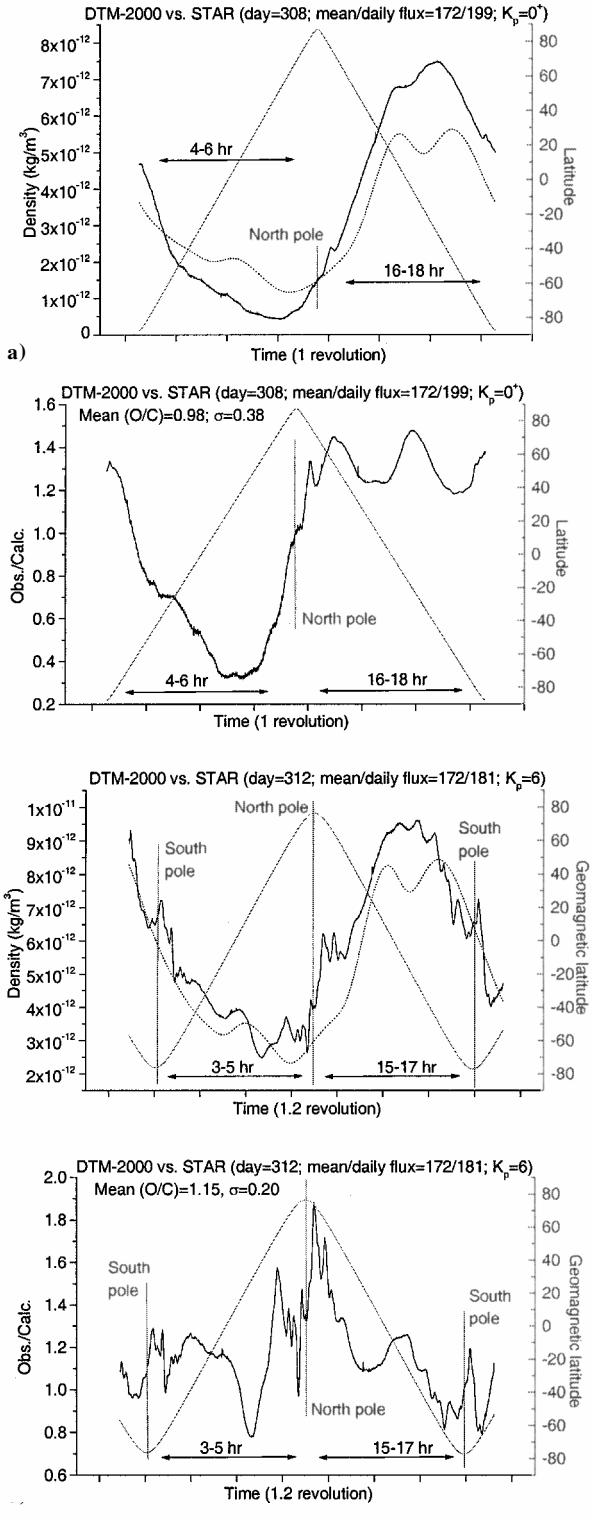

Fig. 5 Observed (——) vs modeled (· · · ·) densities under low and high geomagnetic activity (a and c), and the corresponding O/C (b and d). The local time and the latitude of the profile are equally displayed.

Wind Model) in order to correct our satellite speed modeling, but the resulting densities were only slightly different (<1%) and still presented the large peaks in the auroral regions. The maximum wind predicted by HWM90 was approximately 200 m/s for the orbit used to derive the densities shown in Fig. 5c.

The global statistics concerning the residuals (O/C), their mean, and rms, as well as the range of the mean solar activity, altitude and latitude coverage of the following data sets compared with the models DTM-2000, DTM-94, and MSIS-86 are given in Table 3 for CHAMP/STAR, Dynamics Explorer-2 (DE-2),[14] and CACTUS.[5] The DE-2 data sets provide partial densities, obtained by mass spectrometer measurements, whereas the CACTUS data set concerns total densities derived from accelerometer observations.

DTM-2000, DTM-94, and MSIS-86 have a bias of 17, 18, and 20% with respect to the STAR-derived densities, respectively. This might be caused by an error in the estimated instrumental calibration parameters of STAR or the drag coefficient modeling. Because of calibration problems, a scale factor per constituent has equally been applied to the DE-2 data. These were estimated using a thermospheric model[1,3] instead of under controlled conditions, which explains their small biases. Therefore, the DE-2 densities have uncertainties of the order of 10–20%, and so the STAR residuals might actually reflect the model bias. The DE-2 oxygen data set is comparable in geographical coverage and solar activity range to the STAR data set, but it covers $1\frac{1}{2}$ years instead of six weeks. The rms of the STAR residuals, around 0.3, are higher than the average, and significantly higher than those of DE-2 oxygen (approximately 0.19). Elimination of high latitude data, or of data with $K_p > 3$, did not diminish the rms. Therefore, it is not as a result of unmodeled winds or lesser model accuracy at high latitudes. The last two paragraphs of this section deal with this question. The DE-2 molecular nitrogen data set is noisy, and DTM-2000 reproduces the data with an rms of 26%; the future STAR data, once CHAMP has decayed below 400 km altitude, will increase the coverage of the data and probably improve the modeling accuracy. CACTUS has been included in Table 3 because it is a data set also derived from an accelerometer, although with a limited geographical and solar activity coverage, so that at least for the next few years it remains incompatible with STAR. At the end of the mission, close to solar cycle minimum, the data will be comparable in a clipped latitude interval.

Table 3 seems to indicate that the modeling accuracy is better than 20%; this is not confirmed by STAR data. However, the shorter the time series analyzed, the more important is the proxy used to represent the solar activity in the extreme ultraviolet and ultraviolet (EUV, UV) range. Most upper-atmosphere models use the solar radio flux $F_{10.7}$ because of its long and complete time series (since 1947). However, in a recent study it has been demonstrated that it suffers from several defects as an EUV proxy and that the chromospheric *Mg* II index[4] is more representative of those emissions. This has been shown by constructing two test models under identical conditions and with the same observations, but which were driven by either $F_{10.7}$ or the *Mg* II index.[15] The model employing the *Mg* II index was significantly more accurate, in particular when comparing over small periods of time. The differences between the two indices on timescales of days to several solar rotations are large during high solar activity; when comparing them over an entire solar cycle, on the other hand, their correlation is close to 100%. There is a drawback, however: the *Mg* II index is derived from satellite-borne spectrometer measurements, which are not available on a continuous, daily basis.

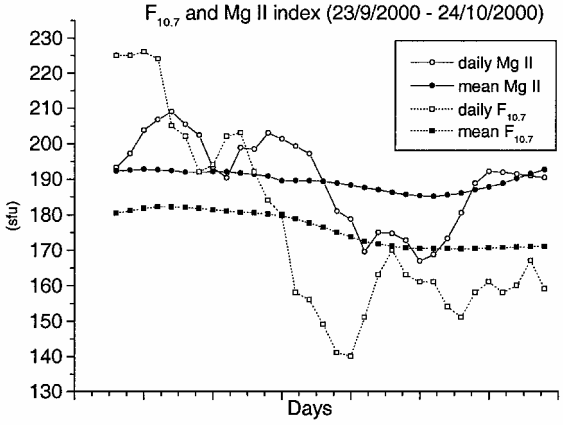

Fig. 6 Solar radio flux $F_{10.7}$ (■, □) compared with the *Mg* II index (●,○) over the analyzed period of six weeks in this study.

The *Mg* II index is available up to 25/10/2000, after which date the mean index is not available until after the period under study now. Thus, we can compare DTM-2000, which was actually based on that index, with the STAR data up to that same date, employing $F_{10.7}$ and the *Mg* II index. The results are convincing: the mean of the residuals decreases from 1.13 to 0.93, and their rms from 0.32 to 0.20, respectively, when using *Mg* II instead of $F_{10.7}$. Figure 6 displays the mean and daily values of the *Mg* II index, converted into $F_{10.7}$ units and $F_{10.7}$. For the period under investigation, the *Mg* II index has a significantly higher mean than $F_{10.7}$, and the daily variations are smaller with respect to the mean. The higher mean value of the *Mg* II index explains the smaller model bias because the density increases with solar activity. The fast variations in the daily radio flux cause equally fast variations in predicted density. These are not well correlated with EUV emissions over the period under study, which explains the higher rms of the residuals.

Conclusions

The analysis of a first CHAMP/STAR density data set showed their potentially large contribution to density modeling: they provide excellent coverage and are precise under low-to-moderate geomagnetic activity. The uncertainty of the retrieved density observations is 15–25% depending on the high-latitude winds, the amplitudes of which increase with geomagnetic activity. Upper-atmosphere neutral wind observations, in particular during geomagnetic storms, must be collected to decrease the uncertainty because empirical wind models are not sufficiently accurate. However, the uncertainty caused by the modeled drag coefficient remains. Simultaneous accelerometer and mass spectrometer observations would make its determination possible, on the condition that both instruments are accurately calibrated. This study also confirmed the better representativity of the *Mg* II index of solar EUV/UV emissions compared with that of $F_{10.7}$. Unfortunately, this index is not available on a continuous, daily basis.

Acknowledgments

The authors acknowledge the entire STAR CAL/VAL team for data-processing support. The thermospheric wind amplitudes used in the error budget were obtained from the CEDAR database.

References

[1]Berger, C., Biancale, R., Ill, M., and Barlier, F., "Improvement of the Empirical Thermospheric Model DTM: DTM94—a Comparative Review of Various Temporal Variations and Prospects in Space Geodesy Applications," *Journal of Geodesy*, Vol. 72, No. 3, 1998, pp. 161–178.

[2]Bruinsma, S. L., and Thuillier, G., "A Revised DTM Atmospheric Density Model: Modelling Strategy and Results," European Geophysical Society XXV General Assembly, Session G7, Nice, France, April 2000.

[3]Hedin, A. E., "MSIS-86 Thermospheric Model," *Journal of Geophysical Research*, Vol. 92, No. A5, 1987, pp. 4649–4662.

[4]DeLand, M. T., and Cebula, R. P., "Composite Mg II Solar Activity Index for Solar Cycles 21 and 22," *Journal of Geophysical Research*, Vol. 98, No. D, 1993, pp. 12,809–12,823.

[5]Villain, J. P., "Traitement des Données Brutes de L'accéléromètre Cactus. Etude des Perturbations de Moyenne Échelle de la Densité Thermosphérique," *Annales Geophysicae*, Vol. 36, No. 1, 1980, pp. 41–49.

[6]Knocke, P. C., Ries, J. C., and Tapley, B. D., "Earth Radiation Pressure Effects on Satellites," *Proceedings of the AIAA/AAS Astrodynamics Specialist Conference*, AIAA, Washington, DC, 1988, pp. 577–587.

[7]Cook, G. E., "Satellite Drag Coefficients," *Planetary and Space Science*, Vol. 13, 1965, pp. 929–946.

[8]Perret, A., Biancale, R., Camus, A. L., Lemoine, J. M., Fayard, T., Loyer, S., Perosanz, F., and Sarrailh, M., "STAR Commissioning Phase Calibration/Validation Activities by CNES," Centre National d'Etudes Spatiales, Rept. DSO/ED/TU/EI 65-2001, Toulouse, France, May 2001.

[9]Biancale, R., Balmino, G., Lemoine, J. M., Marty, J. C., Moynot, B., Barlier, F., Exertier, P., Laurain, O., Schwintzer, P., Reigber, C., Bode, A., König, R., Massmann, F. H., Raimondo, J. C., Schmidt, R., and Zhu, S. Y., "A New Global Earth's Gravity Field Model from Satellite Orbit Perturbations: GRIM5-S1," *Geophysical Research Letters*, Vol. 27, No. 22, 2000, pp. 3611–3614.

[10]Marcos, F. A., Baker, C. R., Bass, J. N., Killeen, T. L., and Roble, R. G., "Satellite Drag Models: Current Status and Prospects," AIAA Paper 93-621, Aug. 1993.

[11]Ferraz-Mello, S., "Estimation of Periods from Unequally Spaced Observations," *Astronomical Journal*, Vol. 5, No. 4, 1981, pp. 619–624.

[12]Menviele, M., and Berthelier, A., "The K-Derived Planetary Indices: Description and Availability," *Reviews of Geophysics*, Vol. 29, No. 3, 1991, pp. 415– 432.

[13]Hedin, A. E., Biondi, M. A., Burnside, R. G., Hernandez, G., Johnson, R. M., Killeen, T. L., Mazaudier, C., Meriwether, J. W., Salah, J. E., Sica, R. J., Smith, R. W., Spencer, N. W., Wickwar, V. B., and Virdi, T. S., "Revised Global Model of Thermosphere Winds Using Satellite and Ground-Based Observations," *Journal of Geophysical Research*, Vol. 96, No. A5, 1991, pp. 7657–7688.

[14]Carignan, G. R., Block, B. P., Maurer, J. C., Hedin, A. E., Reber, C. A., and Spencer, N. W., "The Neutral Mass Spectrometer on Dynamics Explorer," *Space Science Instruments*, Vol. 5, 1981, pp. 429–441.

[15]Thuillier, G., and Bruinsma, S., "The Mg II Index for Upper Atmosphere Modelling," *Annales Geophysicae*, Vol. 19, No. 2, 2001, pp. 219–228.

J. C. Taylor
Associate Editor